# Rab5-mediated Yolk Endocytosis modulates Zebrafish Epiboly Biomechanics and Tissue Movements

**Maria Marsal[*§], Amayra Hernández-Vega[*‡], Philippe-Alexandre Pouille and Enrique Martin-Blanco[#]**

Instituto de Biología Molecular de Barcelona, Consejo Superior de Investigaciones Científicas

Parc Cientific de Barcelona, Baldiri Reixac 10, 08028 Barcelona, Spain

* These authors contribute equally to this work

§ Present address

ICFO - The Institute of Photonic Sciences, Castelldefels, Spain

‡ Present address

Max Planck Institute of Molecular Cell Biology and Genetics (MPI-CBG), Dresden, Germany

# Corresponding author

Enrique Martin-Blanco: embbmc@ibmb.csic.es

## Summary

Morphogenesis in early embryos demands the coordinated allocation of cells and tissues to their final end in a spatio-temporal controlled way. Topographical and scalar differences in adhesion and contractility are essential for these morphogenetic movements, while less clear are the roles that membrane remodeling (reviewed in [1]) may have. To determine how surface turnover may modulate tissue arrangements during embryogenesis we resorted to study epiboly in the zebrafish. Experimental analyses and modeling have shown that the expansion of the blastoderm during epiboly relies on an asymmetry of mechanical tension along the embryo surface [2]. In this scenario, we found that membrane turnover at the external yolk syncitial layer (E-YSL) in early zebrafish is mainly directed by the GTPase *rab5ab*. *rab5ab* was essential for endocytosis, and interference in its expression resulted in reduction of yolk acto-myosin contractility, disruption of cortical and internal flows, a disequilibrium in force balance and epiboly impairment. We conclude that regulated membrane remodelling is crucial for directing cell and tissue mechanics and coordinating morphogenetic movements.

## INTRODUCTION

Membrane turnover might be clathrin-dependent, caveolae-mediated or via macropinocytosis. Clathrin mediated endocytosis (CME), a mechanism for controlled cargo uptake, is the most general membrane internalization route. It is characterised by the formation of clathrin-coated vesicles (CCV) and the selective internalisation of cell-surface components and extracellular macromolecules (for review see [3]). CME depends on dynamin activity for vesicle budding and scission, which leads to trafficking through the endocytic pathway upon clathrin coat disassembling. Caveolae (which incorporate caveolin) are also widely employed by cells for membrane removal. They originate in the Golgi apparatus, associate to cholesterol pools and are involved in the internalization of specific markers and perhaps in transcytosis. Finally, internalization can also take place by macropinocytosis, which usually occurs within highly ruffled regions of the plasma membrane, and is involved in large-scale membrane internalization [4-6]. Macropinocytosis is both Rac1 and actin dependent and many studies have linked it to the ability to form membrane folds. Importantly, Rab5 (usually implicated in CME [7]) and its effector rabankyrin5 are also involved in macropinocytosis [8-10]. Whatever the mechanism of vesicle formation, their trafficking through the endosomal route is controlled by specific Rab guanosine triphosphatases (GTPases): amongst them, Rab5 for internalization and merging into early endosomes; Rab4 for fast recycling towards the plasma membrane; Rab11 for the recycling endosome; and Rab7 for late endosome transport to lysosomes amongst others (reviewed in [11]).

Endocytosis and recycling have been linked in several ways to different cellular maturation (e.g. dendritic arborization in *Drosophila* larvae revealing an important link between microtubule motors and endosomes [12]) or morphogenetic processes affecting the regulation of surface area [13, 14], tension or contraction [15, 16]. Cellularization and Dorsal Closure in *Drosophila* and neurulation and the apical constriction of bottle cells during gastrulation in *Xenopus laevis* are just some examples of processes demanding a tight control of membrane dynamics [14, 17, 18]. Dynamin and Rab5 are necessary downstream of actomyosin contractility to remove excess membrane. Disrupting endocytosis with dominant-negative dynamin or rab5 further perturbs neurulation in Xenopus, inhibiting apical constriction in hingepoint cells and resulting

in neural tube closure defects [14]. Last, Rab5 mediates the cohesion of mesodermal and endodermal (mesendodermal) progenitor cells during zebrafish gastrulation. Endocytosis seems to affect slb/wnt11 activity and Rab5c modulates the ability of cells to aggregate via E-cadherin into distinct clusters, which is necessary for the coordinated movement of the prechordal plate [19]. The modulation of the balance between endocytosis and recycling can regulate cellular morphology and tissue deformations and could be a general mechanism to achieve efficient invagination in embryos.

We aimed to understand the role that membrane remodeling might have during epiboly in zebrafish, a conserved early morphogenetic event. At the onset of zebrafish epiboly (sphere stage), a superficial layer of cells, the enveloping layer (EVL) covers a semi-spherical cap of blastomeres centered on the animal pole of the embryo sitting on a massive yolk syncitial cell. Epiboly consists on the cortical vegetal ward expansion of the EVL, the deep cells (DCs) of the blastoderm and the external layer of the syncytial yolk (E-YSL) around the yolk. Epiboly ends with the closure of the EVL and the DCs at the vegetal pole [20-22] (**Figure 1A**). Epiboly progression associates to a coordinated series of cellular events. EVL cells and DCs proliferate and intercalate resulting in EVL expansion and DCs intercalation and ingression [15, 23]. At the yolk, the E-YSL membrane becomes highly convoluted [24] and gradually narrows by localized contraction [2]. As the EVL margin advances, polymerized actin gets progressively confined to a belt at the animal edge of the E-YSL and to the vegetal cap [23, 25]. In the E-YSL, actin is conscripted within and beneath the highly dynamic convoluted ruffles [2]. Actin accumulation is accompanied by myosin phosphorylation [25]. Remarkably, the narrowing of the E-YSL occurs in synchrony with cortical retrograde actin and myosin flows originating at the vegetal pole [26]. Moreover, internally and coupled to epiboly progression, yolk granules sustain stereotyped dynamic movements [2].

It has been suggested that longitudinal and latitudinal tensional forces originating at the E-YSL constitute the major force-generating elements driving epiboly [23, 25, 27, 28]. It has also been proposed that for the vegetal ward movement of the blastoderm some source of tension must be coupled to the contractile E-YSL. Flow-friction motors could generate a pulling longitudinal force through resistance against the retrograde actomyosin cortical flows in the yolk [26]. Alternatively, a positive vegetal ward oriented latitudinal tension gradient at the yolk membrane from the EVL margin could convey the stress originated by the constriction of the actomyosin ring at the E-YSL [2].

Still, whichever are the mechanical means involved, epiboly must overcome the hindrance that the yolk membrane poses to its progression. The EVL does not slide over the yolk surface and is firmly attached to it [2, 25]. Thus, as it expands, the yolk membrane subsides [15, 23, 27] suggesting that membrane removal at the yolk may constitute an essential event enabling epiboly progression.

To analyze the role of membrane remodeling in the yolk during epiboly we first topographically and temporally characterized its progression as epiboly proceeds. Then, we found that the activity of Rab5ab, a key element of the endosomal route and a mediator of macropinocytosis [11], is essential for yolk membrane turnover and epiboly morphogenetic movements. Indeed, it was previously found that knockdown of *rab5ab* produced a strikinging morphological phenotype during gastrulation [29]. This differs from previous reports interfering on dynamin 2 activity (clathrin-mediated endocytosis) [30], which indicated that the removal of the yolk membrane was dispensable for epiboly. We also found that Rab5ab is essential for the proper recruitment of actin and myosin to the E-YSL and its contractile activity affecting EVL cells elongation and internal yolk flows. Impairing *rab5ab* expression alters the epiboly's biomechanical landscape decreasing the yolk surface tension leading to a reduction on the strength of the E-YSL as a mechanical power source. Summarizing, localized membrane removal in the yolk constitutes a necessary step for epiboly progression bridging cellular, geometrical and mechanical constrains.

## RESULTS

### E-YSL membrane dynamics

To study the zebrafish embryo membrane turnover during epiboly we employed fluorophore-conjugated lectins to label its external membranes. Lectins bind to glycoproteins and glycolipids and have already been used to follow plasma membrane dynamics in other teleost embryos [23]. Upon bathing the embryo in fluorophore-conjugated lectin-containing media, both, the whole yolk and the EVL external membranes were quickly homogeneously decorated. Immediately after, lectin-enriched spots, resembling endocytic vesicles, deposited beneath the yolk membrane,

accumulating in a circumferential ring ahead of the EVL leading cells (**Fig. 1B** and **Movie S1**). Membrane removal ahead of the EVL can be observed as early as the sphere stage and colocalized with the convoluted E-YSL, where actin and myosin progressively gather [26]. We observed a tight spatiotemporal correlation between the narrowing of the endocytic belt and the reduction of the width of the E-YSL (convoluted yolk surface) (**Fig. 1C**), which suggests an intimate relationship between both events. Remarkably, fluid phase endocytosis, reported by the uptake of fluorescent dextran [29, 31], displayed the same pattern as lectin internalization (**Fig. 1D**).

To precisely map and characterize yolk membrane turnover, this was locally tagged by laser photobleaching and its dynamics followed *in vivo*. Membrane photobleached regions away of the EVL edge remained static, indicating the lack of major lateral diffusion within the yolk membrane, up to the time at which the photobleached areas of the yolk got embedded in the advancing E-YSL. At this time the tagged membrane subdued and became endocytosed (**Fig. 1E** and **Movie S2**). The photobleached area linearly reduced its size and was finally eliminated before contacting the EVL margin (**Fig. 1F**).

The observed dynamics of the yolk membrane confirms that the EVL does not slide over the yolk [25] and suggests that its progression demands the graded removal in an animal-vegetal direction of the E-YSL, so that the overall surface of the embryo remains constant.

**Rab5ab-mediated endocytosis is required in the yolk for epiboly progression**

We found that the turnover of the yolk membrane is topographically associated to the E-YSL proximal domain. The extensive convolution of this area points to non-clathrin dependent macropinocytosis as the source of its removal. Indeed, abolishing Dynamin-2 expression in the yolk results in just a partial inhibition of endocytosis not affecting epiboly progression [30].

To fully block endocytosis we resorted in interfering in Rab5 expression, a key element for both vesicle internalization and targeting to early endosomes and macropinocytosis. To target just the yolk without affecting the blastoderm, we performed injections of morpholinos into the yolk (YMOs) at the late 512-1000 cell-stage. In this way, the MOs remained confined to the yolk cell and were not mobilized to the rest of the embryo

[32]. Yolk injection of mRNAs or fluorescently-tagged MOs at these stages showed restricted expression in the yolk (**Fig. S1**).

In zebrafish, there are five annotated *rab5* genes (*rab5aa*, *rab5ab*, *rab5b*, *rab5c* and *rab5clike*). Of these, *rab5aa*, *rab5ab*, and *rab5c* were known to be ubiquitously expressed, unlike *rab5b*, whose expression is limited to the yolk syncytial layer, pronephric duct, and telencephalon [33].

We tested whether inhibition of different *rab5* genes prevented membrane removal by monitoring fluid-phase dextran endocytosis. Three different *rab5ab* morpholinos, Rab5ab YMO1 (splice-blocking), Rab5ab YMO2 and Rab5ab YMO3 (translation-blocking) injected in the yolk all caused the same phenotype, while control mismatch or Rab5c YMOs [34] did not. Rab5ab depletion just in the yolk led to deficient membrane removal (**Fig. 2A** and **Movie S3**). Quantitative analysis further showed that the number of internalized dextran-containing vesicles in Rab5ab YMOs was reduced by 84 % (n = 7), while interfering with the expression of dynamin 2 in the yolk just reduced this figure by 48 % [30].

Importantly, dose dependent Rab5ab yolk depletion resulted in strong early epiboly delay and arrest although other gastrulation and morphogenetic movements (invagination, convergence and extension and somitogenesis) and head and trunk development seemed mostly unaffected initiating timely (as in age-matched control siblings) (see **Fig. 2B** and **Movie S4**). Rab5ab YMOs displayed a dose dependent response. Prior to epiboly no apparent phenotype was observed in any case. However, different degrees of delay were observed from dome stage. At a low dose (4 ng / embryo), Rab5ab YMOs domed in a timed manner but slow down immediately after, halting at 70 % epiboly. When control embryos reached the shield stage, low dose Rab5ab YMOs had not progressed beyond 30 % and when the DCs of controls closed the yolk plug, Rab5ab YMOs remained at 60 % epiboly (compare **Fig. 2C** to **2D**; see **Movie S5**). High dose yolk-injected embryos (8 ng / embryo) consistently showed a strong epiboly delay and never progressed beyond 50 %, when the yolk bursted (compare **Fig. 2C** to **2E**; see **Movie S6**). Epiboly arrest correlated with a progressive folding of the DC layer that detached from the YSL, and with a major constriction at the surface ahead of the EVL margin. Alongside epiboly delay, the Rab5ab YMOs failed to thin the expanding blastoderm, which retracts animalward.

Altogether, these data indicate that *rab5ab* dependent endocytosis is involved in local yolk membrane removal at the E-YSL and that this is necessary to enable epiboly progression.

### *rab5ab* activity in the yolk affects cortical actomyosin and, non-autonomously, EVL shape and yolk granules dynamics

The epiboly progression defects observed upon inhibiting *rab5ab* expression in the yolk were associated to multiple cellular and structural defects. The local recruitment to the E-YSL of actin and activated myosin was compromised by middle dose interference in yolk Rab5ab expression. The levels of both proteins, detected with phalloidin and an anti phospho-myosin antibody, were on average strongly reduced in Rab5ab YMOs (**Fig. 3A** and **3B**). These reductions were linked to defects in the retrograde cortical myosin flow that originates at the vegetal pole and sinks into the E-YSL in wild type embryos [26]. Live time-lapse imaging of transgenic Tg (β-*actin:MYL9L-GFP*) embryos revealed that the magnitude of the yolk cortical myosin flows was reduced and their directionality altered (**Fig. 3C** and **Movie S7**). The narrowing of the actin-rich convoluted E-YSL, the major source of force generation during epiboly [2], was also affected. In these morphants, overtime, the E-YSL got wider (quantified from surface projections of membrane-GFP tagged embryos - see Experimental Procedures) than in wild type (**Fig. 3D**).

These direct effects of interfering in membrane endocytosis on the yolk cortical actomyosin dynamics were accompanied by non-autonomous changes in the shape of EVL cells. EVL cells flattening and elongation (animal to vegetal - AV), which are known outcomes of the accumulation of actin and activated myosin in the E-YSL [25], were prevented in Rab5ab YMOs, where the leading EVL cells elongated in the dorsal to ventral (DV) direction (**Fig. 3E** and **Movie S8**). We reasoned that these altered shapes respond to changes in the tension anisotropy within the E-YSL, which as a rule in normal conditions, increases as epiboly progresses [2].

Last, we found that the stereotyped movements of yolk granules, which passively respond to the cortical stresses at the E-YSL [2], became unbalanced upon *rab5ab* depletion. Velocity fields, estimated by Particle Image Velocimetry (PIV) from meridional multiphoton microscopy sections, showed that the yolk granules regular

toroidal vortices associated to epiboly [2] were completely disrupted (see **Fig. 4A** and **Movie S9**). In Rab5ab YMOs, the yolk granules flows became incoherent showing a noticeably slower kinetics.

In summary, our data indicate that membrane removal at the E-YSL mainly mediated by *rab5ab* is necessary for the correct structural organization and activity of the E-YSL. Endocytic activity in the yolk, ahead of the EVL, would influence E-YSL contractility, which will non-autonomously affect both EVL cells elongation and the pattern of yolk granules flows.

**Epiboly mechanics in Rab5abYMO embryos**

We found that in addition to the structural defects of the E-YSL upon epiboly arrest, the overall geometry of the embryo was affected as a result of the impairment of yolk membrane removal in Rab5ab YMO embryos. The embryos final shape was rather an ellipsoide than a sphere with an elongated animal to vegetal (AV) axis (see **Fig. 2** and **Movie S5**). This elongated shape resulted from both the animalward expansion of the blastoderm after 50 % epiboly and the slight elongation of the yolk towards the vegetal pole. The altered geometry of these embryos suggests that their global biomechanics was compromised and that the topography and dynamics of stresses during epiboly were disrupted. To explore this possibility, we analyzed the spatio-temporal profile of mechanical power and cortical tension of Rab5ab YMOs by Hydrodynamic Regression (HR) [2]. Briefly, throughout epiboly in wild type embryos, HR reveals a stereotyped mechanical power density pattern. At the epiboly onset, the active structures mainly map to the blastoderm. Then, once the EVL crosses the equator, the largest mechanical power density localizes in the active, actomyosin-rich, E-YSL while the adjacent EVL cells opposes deformation. Further, a gradient of tension pointing towards the vegetal pole progressively develops at the yolk surface [2].

As a source to define the biomechanical make up of Rab5ab YMOs versus controls we employed experimental 2D velocity fields obtained by PIV from time-lapse imaging of meridional sections (see above, **Fig. 4A** and **Movie S9**). These analyses neatly showed that the yolk granules' flows were severily impaired (see **Movie S10**). Simulated 3D velocity fields generated from a spherical cortex model were fitted to the experimental velocity fields and dynamic pressure, mechanical power densities and surface tension

maps were all inferred by HR [2]. Through this analysis, we found that while mechanical energy was reduced by four times, the topographical distribution of mechanical power in Rab5ab YMOs was indistinguishable (**Fig. 4B** and **Movie S11**) of that of wild type animals [2]. On the contrary, both longitudinal (AV) and latitudinal (CC) surface stresses and the positive vegetalward gradient of tension in the yolk surface of wild type siblings [2] were significantly decreased in Rab5ab YMOs (see **Fig. 4C** and **Movie S12**). These data indicate that Rab5ab-mediated yolk endocytosis does not influence where and when mechanical power builds up during epiboly but is necessary to reach a proper level of cortical tension.

To validate the tensional topology of the yolk cortex obtained by HR in Rab5ab YMOs we employed laser microsurgery [35]. The experimental disruption of the yolk cortex resulted in immediate recoil with an exponentially decaying speed proportional to the tension present before ablation [36]. We performed laser cuts in the AV direction at the E-YSL of both Rab5ab YMO embryos and controls. These confirmed as an outcome of impaired membrane removal the reduction of surface tension inferred by HR (**Fig. 5A**). Next, by performing laser cuts parallel to the EVL in the yolk cortex at different distances from the EVL margin, we confirmed the predicted absence of a yolk vegetalward gradient of tension in Rab5ab YMOs. The averaged recoil velocities for a series of 20 μm laser cuts performed at 65 % epiboly at 20 μm (n = 21) and at 60 μm (n = 9) ahead of the EVL margin showed no statistically significant differences. On the contrary, in control wild type embryos, stress tension (recoil velocity) increases by 60 % vegetalward between equivalent cuts [2].

All in all, our data indicate that local membrane removal is essential to strength the latitudinal (CC) and longitudinal (AV) forces building up at the E-YSL and for the development of an anisotropic gradient of tension at the cortex. These, jointly, would govern epiboly movements.

## DISCUSSION

The function of plasma membrane remodeling during morphogenesis is recently receiving high attention. It has been shown that Rab5 mediated endocytosis is required

downstream of acto-myosin contraction to remove membrane excess in bottle cells in *Xenopus* and to promote their coordinated constriction [14]. Likewise, Rab5 is required in the amnioserosa during dorsal closure in *Drosophila* prior to cell delaminations to remove membranes as cells delaminate [18]. In zebrafish, different Rab5 isoforms appear to have different roles, participating in nodal signalling in early embryos (*rab5ab*), or muscle and brain development (*rab5b* and *rab5c*) [29]. On the other hand, Rab11 mediated recycling seems to regulate epidermal cells elongation and membrane growth and invagination during cellularization in fly embryos [37]. The balance between endocytosis and recycling seems thus to be critical to regulate cell morphology and tissue deformations in multiple morphogenetic processes.

The contractile capabilities and gradual change of dimensions of the E-YSL along the dissimilar elastic properties of the EVL and the yolk surface minimally account after crossing the equator for epiboly kinematics and mechanical behavior [2]. The proximal E-YSL exerts an isotropic contractile force that generates stress at its adjacent structures, the EVL and the yolk cortex, which have different mechanical properties. The EVL is easily deformed by this pulling force and passively expands. On the opposite, the thin yolk cortex cannot stretch in response to contraction. In this scenario, we propose that membrane (surface area) removal becomes essential for effective movements towards the vegetal pole (**Fig. 5B**). The non-convoluted yolk cortex, accordingly would be progressively recruited to the adjacent E-YSL as this is eliminated.

Endocytosis of the E-YSL surface was previously suggested to contribute to epiboly [15, 27]. However, knock down of Dynamin in the yolk had little effect on epiboly progression [30]. This suggested that the Dynamin-dependent endocytic removal of yolk membrane was dispensable for epiboly. Yet, we found that the depletion of Rab5ab and the subsequent inhibition of endocytosis in the yolk led to epiboly arrest. These opposite results let discard clathrin-mediated endocytosis as the main mechanism involved in membrane trafficking in the E-YSL pointing instead to macropinocytosis. Macropinocytosis is characterized by large non-selective membrane internalization and by the presence of actin cytoskeleton protrusions (ruffles) and has been previously proposed as a plausible mean for membrane remodeling [4-6]. Tipically, the vesicles formed by macropinocytosis are much larger than endosomes (around 0,2 to 0,5 μm) and they seem to be uncoated.

A common underlying feature of endocytic membranes, as opposed to other regions of the plasma membrane, is their high curvature [1]. This curvature is somehow linked to the presence of a specific set of regulatory proteins, many of them necessary for curvature generation [38]. Further, endocytic membrane curvature appears also to be influenced by cytoskeleton motor proteins such as myosin [39]. In addition to pushing forces that might be contributed by actin polymerization (helping, e.g., to push neck membranes closer together), the cytoskeleton may also provide pulling forces to keep vesicles necks under tension [40]. Our data indicate that actomyosin contractility may be necessary at the E-YSL for membrane folding and be initially required to fold the E-YSL membrane into ripples.

While endocytosis of the E-YSL appears to be key for proper epiboly progression, we found that in the absence of Rab5ab, 1) the overall power and the longitudinal and latitudinal stresses (and the shear stress) were severely disturbed and 2) the gradient of tension along the φ axis of the yolk surface was extremely weakened (**Fig. 4C**). As a result the yolk cortical tension, which we validated by laser microsurgery, suffers a significant reduction (**Fig. 5A**). Yet, significant acto-myosin contractile capability persisted and actin and myosin remained localized in the E-YSL cortex in Rab5ab YMOs. Thus, primarily, membrane endocytosis during epiboly appears to follow actomyosin contractility implementing a positive regulatory loop.

Mounting evidences point to a direct relation between membrane reservoir and trafficking pathways with tension in the regulation of cell shape changes and movements in morphogenetic processes [16, 41-47]. During morphogenesis, as tissues change their shapes and sizes, cell membranes dynamically change their area, composition and links to the cortex. As a consequence, membrane tension is subjected to constant modulation [48, 49]. How membrane tension integrates along the cell's overall mechanical properties is unknown. In teleosts, pioneering studies in loach uncovered a direct correlation amongst surface membrane folds and endocytic-rich domains in early eggs. Further, the experimental decrease of loach eggs surface tension by volume reduction was found to lead to a tightly packed folding of their membrane [50]. Alongside, in *Fundulus heteroclitus* embryos, mechanical deformations affect epithelial apical membrane turnover [51]. Yet, these early studies fail to provide a comprehensive view of the links between membrane removal, tension and morphogenetic movements.

We propose that, in the early zebrafish embryo, the surface membrane tension constitutes a mechanical buffering system constantly maintained by endocytosis and contractile activity at the E-YSL that regulates epiboly progression. The rates of removal of the E-YSL membrane would vary with time and will be proportional to the tension of the yolk surface. Endocytosis will lead to membrane tension anisotropies in the yolk surface and these will mechanically feedback to regulate membrane dynamics. This mechanical loop alongside the concerted actions of latitudinal and longitudinal forces at the E-YSL would direct epiboly movements. Mechanical loops set up by membrane remodelling could constitute a common way to coordinate tissue movements in multiple morphogenetic processes

## EXPERIMENTAL PROCEDURES

### Zebrafish lines maintenance

AB and TL wild type strains were used throughout this study. Membrane-GFP transgenic (Tg (β-*actin:m-GFP*)) animals [52] were provided by Lilianna Solnica-Krezel and Myosin-GFP transgenic (Tg (β-*actin:MYL9L-GFP*)) fish (unpublished) were provided by Carl-Philipp Heisenberg. Adult fish were cultured under standard conditions and staged embryos were maintained at 28.5 ºC in embryo medium [53].

### mRNA and Morpholino injections

A DNA construct encoding for LifeAct-GFP [54] and cloned in a Zebrafish expression vector was provided by Erez Raz. mRNA was *in vitro* synthesized (mMessage Machine kit, Ambion) and injected into the yolk at one- or 512-cell stages (150 pg). To knockdown *rab5ab*, morpholino yolk injections (4 ng and 8 ng) were performed at the 512-cell stage.

### Actin, myosin and nuclear stainings

Zebrafish embryos were fixed overnight in 4 % paraformadehyde at 4 °C, washed in 0.3 % Triton in PBS (PBT) and manually dechorionated. They were then washed in PBT,

followed by 2 hours incubation in blocking solution (1 % bovine serum albumin in PBT). Embryos were then incubated either for 1 hour in blocking solution containing 0.2 µg/µl Phalloidin-TRITC (Molecular Probes, Invitrogen) at room temperature or with an antibody against activated myosin (rabbit anti-phospho-myosin light chain 2 Ser19 (Cell Signalling) at 1:100). DAPI was used for nuclear counterstaining. After incubation, embryos were washed 4 times for 15 minutes in PBT. Immunostained embryos were incubated with a secondary fluorescent antibody and washed in PBT. For imaging, embryos were mounted on dishes with 0.5 % low melting agarose in PBS medium. Images were acquired on a Zeiss LSM700 confocal microscope with 10 X / 0.3 and 63 X / 1.40 oil objectives.

**Live Imaging and Analysis**

Whole embryo images were collected from non-dechorionated animals aligned in a 1.2 % agarose mold and covered by E3 medium. Images were acquired (4X magnification) every 5 minutes with an Olympus MVX10 Macroscope.

For confocal and spinning-disc microscopy, embryos were mounted in 0.5 % low melting agarose (A9045 Sigma) in E3 embryo medium.

Sagittal sections (350 µm depth from the yolk membrane surface) were collected from (Tg (β-*actin: m-GFP*)) embryos using a Leica SP5 two-photon microscope equipped with a mode-locked near-infrared MAITAI Laser (Spectra-Physics) tuned at 900 nm, with non-descanned detectors and with a 25 X / 0.95 water-dipping objective. Images were scanned at 200 Hz and frames were averaged three times. Stacks of 30 µm, 10 µm step-size, were acquired every 2 minutes.

Dextran and lectin internalization were monitored from dechorionated embryos previously incubated in 0.05% 10.000 MW Rhodamine B-Dextran (Life Technologies) for 10 minutes [31] or 100µg/ml lectin-TRITC (Sigma L1261) for 5 minutes at the sphere stage, both diluted in E3 embryo medium. The Lectin-TRITC used was from *Helix pomatia* [51], which binds *N*-acetyl-D-galactosamine and *N*-acetyl-D-glucosamine residues of glycoproteins and glycolipids on the cell surface. After treatment embryos were rinsed in E3 medium, mounted in 0.5 % low melting agarose and imaged in a Zeiss LSM700 confocal microscope with a 40 X / 1.3 oil immersion objective. A stack of 20 µm, 0.39 µm step size, was acquired every 4 minutes.

To visualize myosin cortical flows, spinning-disc images were captured from (Tg (β-*actin: MYL9L-GFP*)) embryos on either an Olympus X81 inverted microscope (Andor Technologies), using a 40 X / 0.60 Dry objective or a Zeiss Axiovert 200M inverted microscope (PerkinElmer UltraView ERS) using a 40 X / 1.3 oil DIC objective. Stacks of 16 µm, step size 1 µm, were acquired every 45 seconds.

To visualize the surface of the yolk, (Tg (β-*actin: m-GFP*)) embryos were imaged in a Zeiss LSM700 confocal microscope with a 63 X / 1.4 oil objective. A stack of 25 µm, step size of 0.2 µm was acquired. We also used embryos injected with LifeAct-GFP at the 512-cell stage, collecting the images with a Zeiss Axiovert 200M inverted microscope (PerkinElmer UltraView ERS) using a 100 X / 1.4 oil DIC objective. Stacks of 10µm, step size of 0.45 µm, were acquired every 12 seconds.

For photo-bleaching, selected ROIs were created for lectin-TRITC soaked embryos and bleached using 100 % power of a 555 nm laser with 100 iterations in the selected area (in the YSL at 150 µm from the EVL margin) in embryos at 40 % epiboly. A stack of 4 µm, step size 1 µm, was acquired every 30 seconds.

Most image analyses and processing were performed using Fiji (http://pacific.mpi-cbg.de) and Matlab (Mathworks). To obtain velocity fields we applied the MatPIV software package written by Johan Kristian Sveen for use with Matlab [55]. To measure the width of the wrinkled area, surface projections at different stages were obtained with Matlab and mean width and standard deviations were plotted (Excel, MS Office). To quantify endocytosis, E-YSL dextran-containing vesicles were monitored from maximum projections of Z-stack images.

Laser Surgery Experiments, Retraction Analysis and Hydrodynamic Regression (HR) are described in the Supplemental Experimental Procedures.

## ACKNOWLEDGEMENTS

We thank the Confocal Microscopy Unit from IBMB-PCB, the Advanced Digital Microscopy Core Facility from IRB Barcelona, Xavier Esteban and members of the laboratory for continuous support. We are grateful to Nadine Peyrieras, Lila Solnica-Kretzel and Carolina Minguillón for reading earlier versions of this manuscript. The

Consolidated Groups Program of the Generalitat de Catalunya and DGI and Consolider Grants from the Ministry of Economy and Competitivity of Spain to EMB supported this work.

## AUTHOR CONTRIBUTION

MM and AHV performed all biological tests; PAP designed the modeling and the regression analysis and EMB designed the study, analyzed the data and wrote the paper. MM and AHV contributed equally to the study. All authors discussed the results and commented on the manuscript.

## COMPETING FINANCIAL INTERESTS

The authors declare no competing financial interests.

## REFERENCES

1. Doherty, G.J., and McMahon, H.T. (2009). Mechanisms of endocytosis. Annu Rev Biochem *78*, 857-902.
2. Hernandez-Vega, A., Marsal, M., Pouille, P.A., Tosi, S., Colombelli, J., Luque, T., Navajas, D., Pagonabarraga, I., and Martin-Blanco, E. (2016). Polarized cortical tension drives zebrafish epiboly movements. EMBO J.
3. McMahon, H.T., and Boucrot, E. (2011). Molecular mechanism and physiological functions of clathrin-mediated endocytosis. Nat Rev Mol Cell Biol *12*, 517-533.
4. Lim, J.P., and Gleeson, P.A. (2011). Macropinocytosis: an endocytic pathway for internalising large gulps. Immunol Cell Biol *89*, 836-843.
5. Cao, H., Chen, J., Awoniyi, M., Henley, J.R., and McNiven, M.A. (2007). Dynamin 2 mediates fluid-phase micropinocytosis in epithelial cells. J Cell Sci *120*, 4167-4177.
6. Swanson, J.A., and Watts, C. (1995). Macropinocytosis. Trends in cell biology *5*, 424-428.

7. Zeigerer, A., Gilleron, J., Bogorad, R.L., Marsico, G., Nonaka, H., Seifert, S., Epstein-Barash, H., Kuchimanchi, S., Peng, C.G., Ruda, V.M., et al. (2012). Rab5 is necessary for the biogenesis of the endolysosomal system in vivo. Nature *485*, 465-470.
8. Barbieri, M.A., Fernandez-Pol, S., Hunker, C., Horazdovsky, B.H., and Stahl, P.D. (2004). Role of rab5 in EGF receptor-mediated signal transduction. Eur J Cell Biol *83*, 305-314.
9. Lanzetti, L., Palamidessi, A., Areces, L., Scita, G., and Di Fiore, P.P. (2004). Rab5 is a signalling GTPase involved in actin remodelling by receptor tyrosine kinases. Nature *429*, 309-314.
10. Tall, G.G., Barbieri, M.A., Stahl, P.D., and Horazdovsky, B.F. (2001). Ras-activated endocytosis is mediated by the Rab5 guanine nucleotide exchange activity of RIN1. Dev Cell *1*, 73-82.
11. Zerial, M., and McBride, H. (2001). Rab proteins as membrane organizers. Nat Rev Mol Cell Biol *2*, 107-117.
12. Satoh, D., Sato, D., Tsuyama, T., Saito, M., Ohkura, H., Rolls, M.M., Ishikawa, F., and Uemura, T. (2008). Spatial control of branching within dendritic arbors by dynein-dependent transport of Rab5-endosomes. Nat Cell Biol *10*, 1164-1171.
13. Lecuit, T., and Pilot, F. (2003). Developmental control of cell morphogenesis: a focus on membrane growth. Nat Cell Biol *5*, 103-108.
14. Lee, J.Y., and Harland, R.M. (2010). Endocytosis is required for efficient apical constriction during Xenopus gastrulation. Current biology : CB *20*, 253-258.
15. Betchaku, T., and Trinkaus, J.P. (1986). Programmed endocytosis during epiboly of Fundulus heteroclitus. American zoologist *26*, 7.
16. Gauthier, N.C., Masters, T.A., and Sheetz, M.P. (2012). Mechanical feedback between membrane tension and dynamics. Trends in cell biology *22*, 527-535.
17. Fabrowski, P., Necakov, A.S., Mumbauer, S., Loeser, E., Reversi, A., Streichan, S., Briggs, J.A., and De Renzis, S. (2013). Tubular endocytosis drives remodelling of the apical surface during epithelial morphogenesis in Drosophila. Nat Commun *4*, 2244.
18. Mateus, A.M., Gorfinkiel, N., Schamberg, S., and Martinez Arias, A. (2011). Endocytic and recycling endosomes modulate cell shape changes and tissue behaviour during morphogenesis in Drosophila. PloS one *6*, e18729.
19. Ulrich, F., Krieg, M., Schotz, E.M., Link, V., Castanon, I., Schnabel, V., Taubenberger, A., Mueller, D., Puech, P.H., and Heisenberg, C.P. (2005). Wnt11 functions in gastrulation by controlling cell cohesion through Rab5c and E-cadherin. Dev Cell *9*, 555-564.
20. Solnica-Krezel, L. (2006). Gastrulation in zebrafish -- all just about adhesion? Curr Opin Genet Dev *16*, 433-441.
21. Kimmel, C.B., Ballard, W.W., Kimmel, S.R., Ullmann, B., and Schilling, T.F. (1995). Stages of embryonic development of the zebrafish. Dev Dyn *203*, 253-310.
22. Rohde, L.A., and Heisenberg, C.P. (2007). Zebrafish gastrulation: cell movements, signals, and mechanisms. Int Rev Cytol *261*, 159-192.
23. Cheng, J.C., Miller, A.L., and Webb, S.E. (2004). Organization and function of microfilaments during late epiboly in zebrafish embryos. Dev Dyn *231*, 313-323.

24. Betchaku, T., and Trinkaus, J.P. (1978). Contact relations, surface activity, and cortical microfilaments of marginal cells of the enveloping layer and of the yolk syncytial and yolk cytoplasmic layers of fundulus before and during epiboly. The Journal of experimental zoology *206*, 381-426.
25. Koppen, M., Fernandez, B.G., Carvalho, L., Jacinto, A., and Heisenberg, C.P. (2006). Coordinated cell-shape changes control epithelial movement in zebrafish and Drosophila. Development *133*, 2671-2681.
26. Behrndt, M., Salbreux, G., Campinho, P., Hauschild, R., Oswald, F., Roensch, J., Grill, S.W., and Heisenberg, C.P. (2012). Forces driving epithelial spreading in zebrafish gastrulation. Science *338*, 257-260.
27. Solnica-Krezel, L., and Driever, W. (1994). Microtubule arrays of the zebrafish yolk cell: organization and function during epiboly. Development *120*, 2443-2455.
28. Schepis, A., Sepich, D., and Nelson, W.J. (2012). alphaE-catenin regulates cell-cell adhesion and membrane blebbing during zebrafish epiboly. Development *139*, 537-546.
29. Kenyon, E.J., Campos, I., Bull, J.C., Williams, P.H., Stemple, D.L., and Clark, M.D. (2015). Zebrafish Rab5 proteins and a role for Rab5ab in nodal signalling. Dev Biol *397*, 212-224.
30. Lepage, S.E., Tada, M., and Bruce, A.E. (2014). Zebrafish Dynamin is required for maintenance of enveloping layer integrity and the progression of epiboly. Dev Biol *385*, 52-66.
31. Feng, B., Schwarz, H., and Jesuthasan, S. (2002). Furrow-specific endocytosis during cytokinesis of zebrafish blastomeres. Exp Cell Res *279*, 14-20.
32. Kimmel, C.B., and Law, R.D. (1985). Cell lineage of zebrafish blastomeres. II. Formation of the yolk syncytial layer. Dev Biol *108*, 86-93.
33. Thisse, B., Heyer, V., Lux, A., Alunni, V., Degrave, A., Seiliez, I., Kirchner, J., Parkhill, J.P., and Thisse, C. (2004). Spatial and temporal expression of the zebrafish genome by large-scale in situ hybridization screening. Methods Cell Biol *77*, 505-519.
34. Ulrich, F., and Heisenberg, C.P. (2008). Probing E-cadherin endocytosis by morpholino-mediated Rab5 knockdown in zebrafish. Methods Mol Biol *440*, 371-387.
35. Colombelli, J., Besser, A., Kress, H., Reynaud, E.G., Girard, P., Caussinus, E., Haselmann, U., Small, J.V., Schwarz, U.S., and Stelzer, E.H. (2009). Mechanosensing in actin stress fibers revealed by a close correlation between force and protein localization. J Cell Sci *122*, 1665-1679.
36. Grill, S.W. (2011). Growing up is stressful: biophysical laws of morphogenesis. Curr Opin Genet Dev *21*, 647-652.
37. Pelissier, A., Chauvin, J.P., and Lecuit, T. (2003). Trafficking through Rab11 endosomes is required for cellularization during Drosophila embryogenesis. Current biology : CB *13*, 1848-1857.
38. Kozlov, M.M., Campelo, F., Liska, N., Chernomordik, L.V., Marrink, S.J., and McMahon, H.T. (2014). Mechanisms shaping cell membranes. Curr Opin Cell Biol *29*, 53-60.
39. Spudich, G., Chibalina, M.V., Au, J.S., Arden, S.D., Buss, F., and Kendrick-Jones, J. (2007). Myosin VI targeting to clathrin-coated structures and dimerization is mediated by binding to Disabled-2 and PtdIns(4,5)P2. Nat Cell Biol *9*, 176-183.

40. Roux, A., Uyhazi, K., Frost, A., and De Camilli, P. (2006). GTP-dependent twisting of dynamin implicates constriction and tension in membrane fission. Nature *441*, 528-531.
41. Kremnyov, S.V., Troshina, T.G., and Beloussov, L.V. (2012). Active reinforcement of externally imposed folding in amphibians embryonic tissues. Mech Dev *129*, 51-60.
42. Diz-Munoz, A., Fletcher, D.A., and Weiner, O.D. (2013). Use the force: membrane tension as an organizer of cell shape and motility. Trends in cell biology *23*, 47-53.
43. Apodaca, G. (2002). Modulation of membrane traffic by mechanical stimuli. American journal of physiology. Renal physiology *282*, F179-190.
44. Gauthier, N.C., Fardin, M.A., Roca-Cusachs, P., and Sheetz, M.P. (2011). Temporary increase in plasma membrane tension coordinates the activation of exocytosis and contraction during cell spreading. Proceedings of the National Academy of Sciences of the United States of America *108*, 14467-14472.
45. Dai, J., and Sheetz, M.P. (1995). Regulation of endocytosis, exocytosis, and shape by membrane tension. Cold Spring Harbor symposia on quantitative biology *60*, 567-571.
46. Dai, J., Sheetz, M.P., Wan, X., and Morris, C.E. (1998). Membrane tension in swelling and shrinking molluscan neurons. The Journal of neuroscience : the official journal of the Society for Neuroscience *18*, 6681-6692.
47. Sheetz, M.P., and Dai, J. (1996). Modulation of membrane dynamics and cell motility by membrane tension. Trends in cell biology *6*, 85-89.
48. Figard, L., and Sokac, A.M. (2014). A membrane reservoir at the cell surface: unfolding the plasma membrane to fuel cell shape change. Bioarchitecture *4*, 39-46.
49. Clark, A.G., Wartlick, O., Salbreux, G., and Paluch, E.K. (2014). Stresses at the cell surface during animal cell morphogenesis. Current biology : CB *24*, R484-494.
50. Ivanenkov, V.V., Meshcheryakov, V.N., and Martynova, L.E. (1990). Surface polarization in loach eggs and two-cell embryos: correlations between surface relief, endocytosis and cortex contractility. The International journal of developmental biology *34*, 337-349.
51. Fink, R.D., and Cooper, M.S. (1996). Apical membrane turnover is accelerated near cell-cell contacts in an embryonic epithelium. Dev Biol *174*, 180-189.
52. Cooper, M.S., Szeto, D.P., Sommers-Herivel, G., Topczewski, J., Solnica-Krezel, L., Kang, H.C., Johnson, I., and Kimelman, D. (2005). Visualizing morphogenesis in transgenic zebrafish embryos using BODIPY TR methyl ester dye as a vital counterstain for GFP. Dev Dyn *232*, 359-368.
53. Westerfield, M. (2000). The Zebrafish Book: A Guide for the Laboratory Use of Zebrafish (Danio rerio), (Eugene, OR: University of Oregon Press).
54. Riedl, J., Crevenna, A.H., Kessenbrock, K., Yu, J.H., Neukirchen, D., Bista, M., Bradke, F., Jenne, D., Holak, T.A., Werb, Z., et al. (2008). Lifeact: a versatile marker to visualize F-actin. Nat Methods *5*, 605-607.
55. Supatto, W., Debarre, D., Moulia, B., Brouzes, E., Martin, J.L., Farge, E., and Beaurepaire, E. (2005). In vivo modulation of morphogenetic movements in Drosophila embryos with femtosecond laser pulses. Proceedings of the National Academy of Sciences of the United States of America *102*, 1047-1052.

## FIGURES

### Figure 1

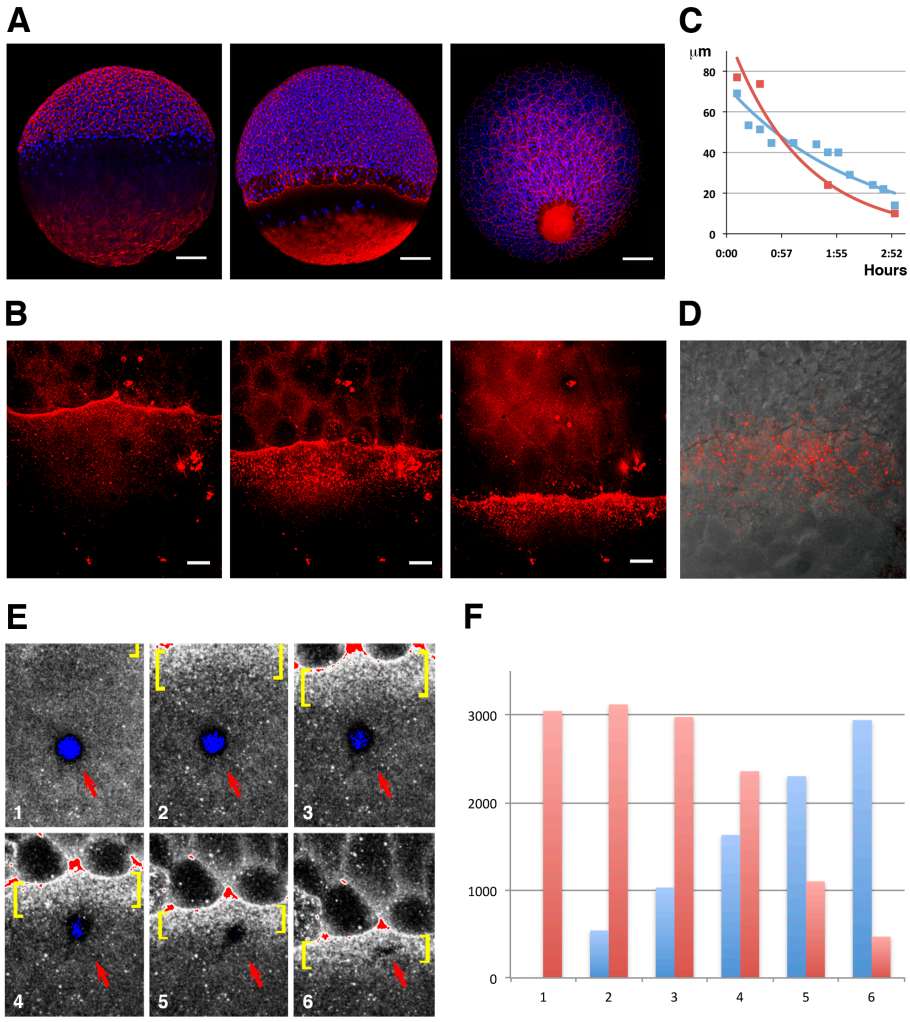


**Figure 1. Yolk membrane endocytosis at the E-YSL**

**A)** Blastoderm expansion during epiboly. At sphere stage epiboly has not yet begun (left). F-actin accumulates at the periphery of all cells as well as in the yolk, mainly at the vegetal cap. At 70 % epiboly (middle), the blastoderm has crossed the equator and will decrease its margin until closure. A belt of actin develops at the E-YSL ahead of the EVL and an actin-free zone separates this belt from a vegetal actin-rich patch. At 90

% epiboly (right), the E-YSL and the vegetal actin-rich patch merge. Embryos were stained with phalloidin-TRITC (red) and DAPI (blue). Scale bars 100 µm. **B**) Sequential images of a confocal time-lapse video of a wild type embryo soaked in lectin–TRITC for 5 minutes at sphere stage. The lectin binds to the membrane of both the yolk and the EVL cells and gets internalized accumulating in vesicles in the E-YSL just ahead of the EVL margin (from **Movie S1**). Scale bar 25 µm. All confocal images are maximum projections. **C)** Parallel reduction during epiboly progression of the width of the convoluted domain (blue) and of the area undergoing membrane removal (red) of the E-YSL. X and Y axes represent hours after 50 % epiboly and width in µm, respectively. **D)** Uptake of fluorescent dextran (red) at the E-YSL just ahead of the EVL margin at 65 % epiboly. **E**) Snapshots of time-lapse images (from **Movie S2**) of a lectin-TRITC soaked embryo showing a circular photobleached area (red arrow) in the yolk away from the EVL leading edge. The photobleached membrane is removed and endocytosed only upon its enclosure within the advancing E-YSL (yellow brackets). All confocal images are maximum projections. Scale bar 25 µm. **F**) Membrane internalization dynamics. Histograms depicting the normalized relationship between the photobleached areas (red) and the progression of the leading EVL front (blue) at regular sequential time points (from 1 in **E**). The removal of the photobleached membrane shows a precise linear relationship with the speed of advancement of the leading front.

**Figure 2**

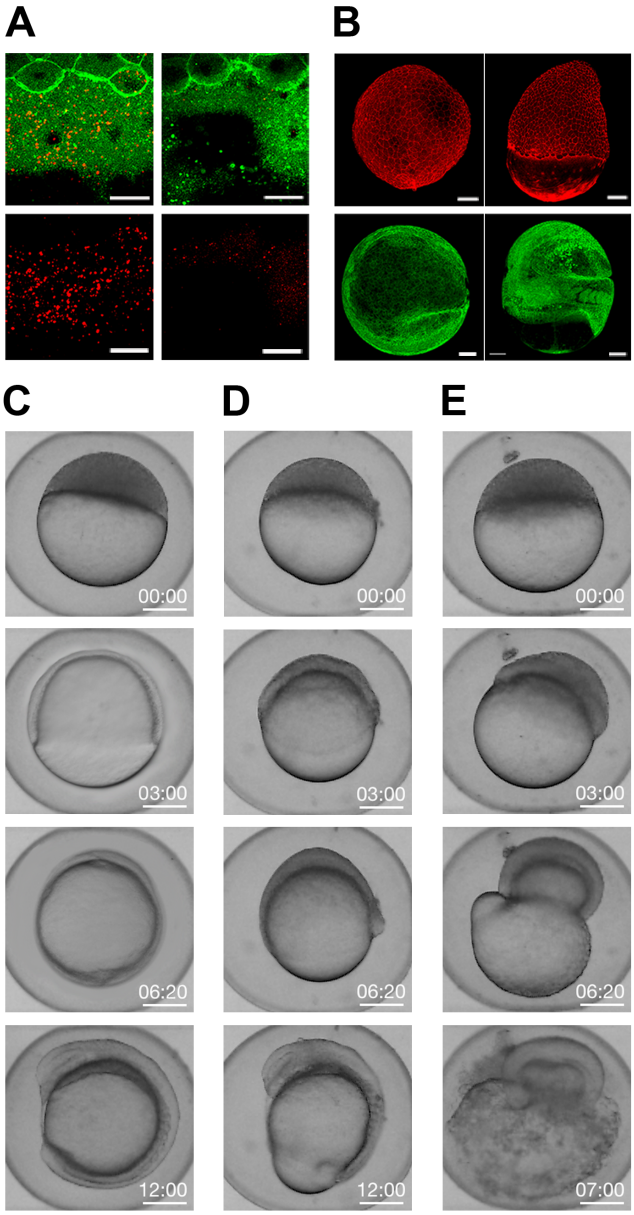


**Figure 2. Endocytosis and Epiboly are impaired by Rab5ab depletion**

**A**) Rhodamine B-Dextran internalization was reduced at doming stage in membrane-GFP (Tg (β-*actin:m-GFP) rab5ab* (right) compared to sibling controls (left) YMOs. Top panels show dextran (red) and membrane staining (green) overlays. Images are confocal maximum projections. Scale bar 25 µm. See also **Movie S3**. **B**) Yolk depletion

of Rab5ab results in epiboly delay without affecting other gastrulation movements [Control (left) and *rab5ab* YMOs (right)]. Top panels show Phalloidin-TRITC (red) staining of a control YMO at the end of epiboly and a sibling medium dose *rab5ab* YMOs of the same age. Lateral views. Bottom pannels show membrane-GFP (Tg (β-*actin:m-GFP*). YMOs at 1 day post fertilization. Rab5ab morphants present an open back phenotype but succeed in other gastrulation movements leading to somite formation (see also **Movie S4**). Images are confocal maximum projections. Scale bar 100 µm. **C-E**) Yolk morphants show a dose dependent epiboly delay. Macroscopic bright field images of sibling controls (**C**) and medium (4 ng) (**D**) and high (8 ng) dose (**E**) *rab5ab* YMOs (from **Movies S5** and **S6**). Medium and high dose morphants remained at 70 and 40 % epiboly respectively when control siblings have already closed. Embryos were imaged in their chorion. Scale bar 250 µm.

## Figure 3

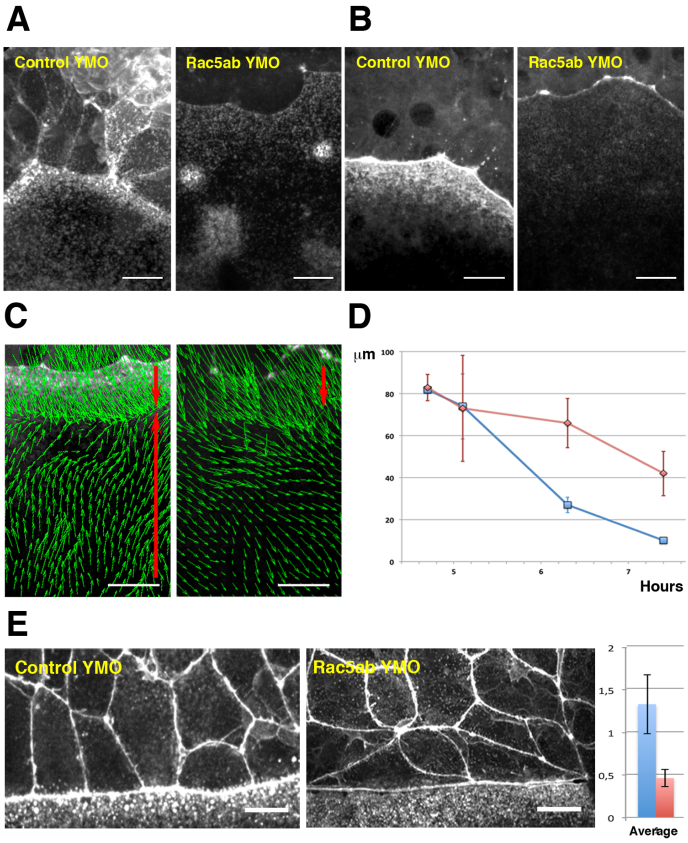


**Figure 3. Cytoskeleton dynamics and EVL leading cells shapes are affected by Rab5ab depletion**

**A)** Actin fails to accumulate at the E-YSL in *rab5ab* YMOs versus controls (C YMO). Time-lapse snapshots of two LifeAct GFP injected sibling embryos. **B)** Myosin fails to accumulate at the E-YSL of *rab5ab* YMOs versus controls (C YMO). Time-lapse snapshots of two Myosin-GFP transgenic (Tg (β-*actin:MYL9L-GFP*)) sibling embryos. Notice the delay in the progression of the EVL and the weaker accumulation of actin and myosin in the *rab5ab* YMOs. **C**) Myosin cortical retrograde flows. PIV of time-lapse snapshots of Tg (β-*actin:MYL9L-GFP*) embryos at 40 % epiboly (from **Movie**

**S7**). Notice the vegetalward movement of cells and E-YSL (red top arrows) and the retrograde animalward cortical flow from the yolk vegetal pole sinking at the E-YSL (red bottom arrows). Scale bar 25 µm. **D**) E-YSL contraction is delayed in *rab5ab* YMOs. Between 4.5 to 7.5 hours post fertilization, the E-YSL width is reduced from 80 to 10 µm as an average in controls (blue), but from 80 to 40 µm in *rab5ab* YMOs (red). Data collected form surface projections of membrane-GFP (Tg (β-*actin:m-GFP*) *rab5ab* and sibling YMOs (see **Movie S8**). **E)** Compared to control siblings at 70 % epiboly (C YMO - left), leading EVL cells of Rab5ab YMOs flatten and elongate latitudinally (right). Actin was stained with phalloidin-TRITC. Scale bars 25 µm. All confocal images are maximum projections. Quantification of the shape ratio (animal to vegetal vs latitudinal - Y axis) of leading EVL cells (far right) show that control siblings (red) are extremely elongated on the animal vegetal direction while leading EVL cells in Rab5ab YMOs (blue) flatten at their front and elongate latitudinally. Standard deviations are shown.

## Figure 4

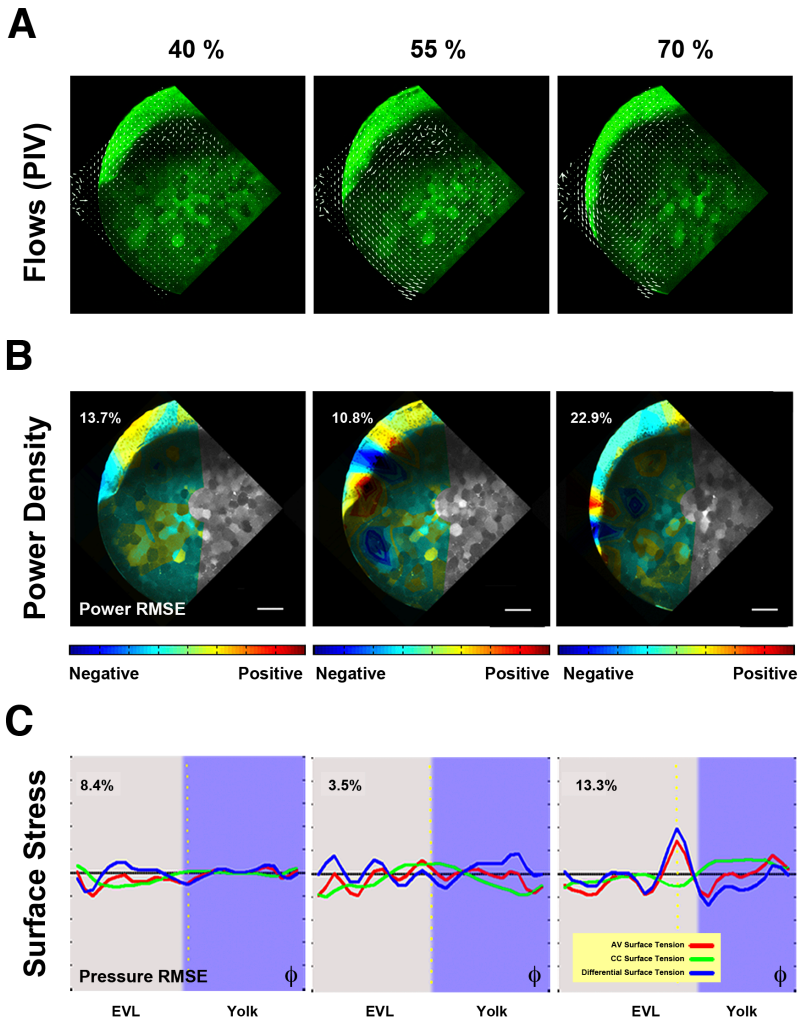


**Figure 4. Biomechanics of yolk endocytosis impaired embryos**

**A**) Yolk granules flows patterns are altered in Rab5ab YMOs. PIV of time-lapse snapshots imaged by two-photon microscopy of a Tg (β-*actin:m-GFP*) Rab5ab YMO (from **Movie S9**; see also **Movie S10**). From epiboly onset, yolk granules flows are imprecise in Rab5ab YMOs. The internal toroidal vortices characteristic of epiboly progression [2] do not form or are severely reduced and the laminar flows become asymmetrically distributed. Animal (A) and vegetal (V) poles are indicated. Scale bar

25 µm. **B**) Mechanical power density maps over time obtained by HR analysis in in *rab5ab* yolk morphants (from **Movie S11**). The RMSE of the power is shown as a percentage. Qualitatively, *rab5ab* YMOs display no differences with wild type embryos in the spatial and temporal distribution of mechanical work [2] but exhibit an overall decrease of power of about four fold. **C**) Longitudinal (red) and latitudinal (green) stresses and their differences (blue) along the embryo cortex in a membrane-GFP transgenic (Tg (β-*actin:m-GFP*)) Rab5ab YMO (from **Movie S12**). Stresses were plotted as a function of the φ angle from animal to vegetal (40 %; 50 %; 65 % epiboly). The equator - dotted yellow line -, yolk surface - purple shadow - and the RMSE of the dynamic pressure as a percentage for each time point are displayed. The latitudinal stress does not steep up from animal to vegetal until 60 % epiboly, while the longitudinal stress oscillations are sustained.

## Figure 5

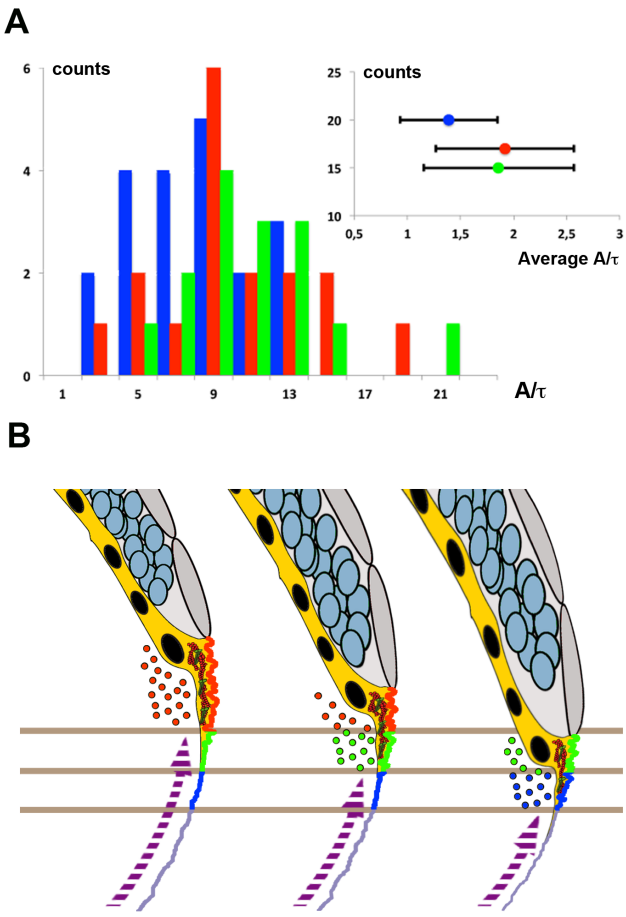


**Figure 5. Membrane cortical tension and endocytosis at the E-YSL are necessary for epiboly progression**

**A)** The distribution (counts) of instant retraction velocities (A/t) after laser surgery of the actomyosin cortex of Myosin-GFP (Tg (β-*actin:MYL9L-GFP*) *rab5ab* YMOs at 55% epiboly (blue) shows a significant reduction (Wilcoxon test $p<0.01$) versus wild type (red) and control morphants (green). The instant velocity estimate was extracted from the exponential fit of the distance between fronts (see Supplemental Experimental

Procedures). The averaged instant retraction velocity (A/t) for *rab5ab* YMOs was 1.39 ± 0.46 mm, while control YMOs reach 1.86 ± 0.71 mm and wild type embryos 1.92 ± 0.65 mm (inset). Counts represent the number of analyzed laser cuts for each condition. **B)** Proposed model of epiboly progression. The contractile E-YSL and the imbalance of stiffness between the EVL and the yolk surface account for epiboly progression. Passive movements within the yolk arise as a result of force transmission from the surface. Rab5ab-mediated yolk localized endocytosis (color coded dots) accounts for the reduction of the yolk surface coupled to the progression of EVL (grey) and DCs (blue) towards the vegetal pole. Membrane removal associates to the convolution of the E-YSL surface and the recruitment of actin and myosin (purple dashed arrow) from vegetally located pools. Three chronological time points are shown. Different sequential zones on the surface of the E-YSL are color-coded. Actin and myosin are diagramatically illustrated in red and green within the YSL (yellow).

# SUPPLEMENTAL EXPERIMENTAL PROCEDURES AND INFORMATION



# SUPPLEMENTAL EXPERIMENTAL PROCEDURES

## Morpholinos

Morpholinos (MOs) were purchased from Gene Tools and designed against selected regions (ATG or UTR) of the *rab5ab* gene (Accession Number ENSDARG00000007257) (Gene Tools): *rab5ab* MO-ATG (5-TCGTTGCTCCACCT-CTTCCTGCCAT-3), *rab5ab* MO-UTR (5-GACCCAAAACCCCAATCTCCTGTAC-3), *rab5ab* MO-UTR-ATG (5-ACCTCTTCCTGCCATGACCCAAAAC-3) and a *rab5ab* mismatch MO (5-TCcTTcCTCgACCTCTTCgTcCCAT-3) (mispaired nucleotides in lower case). Interference with *rab5c* (ENSDARG00000026712)] was performed with the following MO: 5-CGCTGGTC-CACCTCGCCCCGCCATG-3

provided by C.P. Heisenberg [34]. For all experiments, a group of embryos was injected with a Standard Control MO (5-CCTCTTACCTCAGTTACAATTTATA-3).

**Hydrodynamics Regression (HR)**

HR is based in fitting analytically modeled velocity fields to experimental velocity fields in and outside a cortex. Considering that in deforming tissues, stresses at the fluid/cortex boundary are continuous (boundary condition), HR can estimate cortical stresses and retrieve the complete dynamic pressure distribution in the fluid and at the fluid-cortex interface. From these, HR also infers at each time point the cortex shear stress at each point of the surface and the mechanical power density. HR is performed independently at each time point to retrieve the overall spatio-temporal distribution of all these mechanical quantities [2].

In our analyses, experimental 2D velocity fields were estimated by PIV from time-lapse imaging of meridional sections of zebrafish embryos. Second, simulated 3D velocity fields generated from a spherical cortex model (SC) with Stokeslets pairs distributed on a single spherical shell were fitted to the experimental velocity fields. Last, knowing the fluid deformation rates, it is possible to calculate the local values of the cortical surface tension, the cortical mechanical power density and the spatio-temporal evolution of both cortical stresses and mechanical power density maps (analytical codes are available on [2]).

**Laser Surgery Experiments and Retraction Analysis**

Laser surgery of the actomyosin cortex was performed with a pulsed UV laser (355 nm, 470 ps per pulse) by inducing plasma-mediated ablation as described before [35]. To compare the cortical tension in the longitudinal direction at the E-YSL a 20 μm-laser line containing 50 pulses was scanned 5 times at a frequency of 500 Hz, parallel to the EVL front, centering the cut at a distance of about 20 μm, through a 63 X / 1.2 W objective lens. Fluorescence imaging was performed through a custom spinning Nipkow disc unit equipped with a 488 nm laser line and a Hamamatsu ORCA CCD camera, acquiring at 1.5 frames per second. Transmission and fluorescence imaging was performed by alternated illumination with two out-of-phase mechanical shutters blocking the 488 nm laser and the halogen bright field lamp.

We followed the accepted assumption [36] that the tension present in the actomyosin cortex before the laser cut is proportional to the outward velocity of the immediate recoil. Retraction analysis was performed through a customized kymograph analysis along the retraction axis (perpendicular to the cut), with ImageJ (http://rsbweb.nih.gov/ij/). Kymograph processing included subtraction of the intensity minimum and normalization to the maximum, both measured in the position of the cut, to ensure stable edge detection by intensity threshold across the whole sequence. The front-to-front length, during the retraction phase (until reaching a plateau), was fitted to an exponential function (Igor Pro 6.0, Wavemetrics) to evaluate the slope at the origin. The function used was:

$$F(t) = y0 + A\,(1 - \exp(-t / \tau))$$

and the slope at the origin was derived from its derivative:

$$dF(0) / dt = A / \tau$$

The width of photo bleaching (about 1µm) introduced by the UV laser was subtracted to the measured length L. This method was applied to the comparative analysis of morphant conditions.

## SUPPLEMENTAL FIGURES

### Figure S1

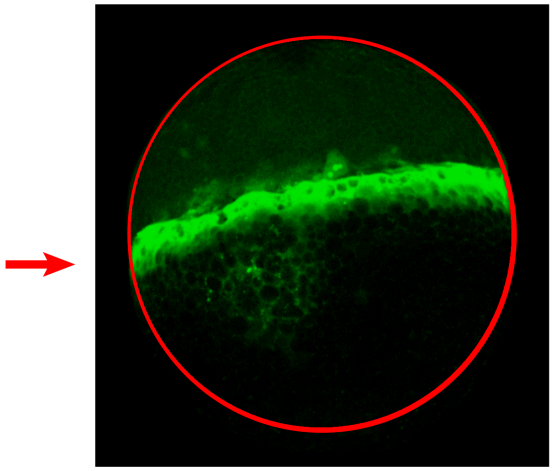

**Figure S1. Yolk-Specific Morphants**

Fluorescent image of an embryo injected at the 512 cells stage with a fluorescently labelled Morpholino (FITC) observed at 40 % Epiboly. The red arrow points to the fluorescence in the yolk, accumulating at the E-YSL.

## SUPPLEMENTAL MOVIES LEGENDS

### Movie S1. Endocytosis

Confocal video time-lapse of a wild type animal soaked in lectin–TRITC for 5 minutes at sphere stage. 20 µm width stacks were captured every 4 minutes. Note the cumulative lectin-TRITC internalization at the E-YSL domain ahead of the advancing EVL.

### Movie S2. Endocytosis at the E-YSL

HiLo LUT code (Fiji) processed confocal video time-lapse of a lectin-TRITC soaked embryo showing a circular photo bleached ROI in the yolk 60 µm away from the EVL leading edge. 4 µm width stacks were captured every 30 seconds. Maximum projection is shown. Scale bar 25 µm. The photo-bleached membrane (blue circle) is not removed or endocytosed and remains unchanged up to its enclosure within the advancing E-YSL.

### Movie S3. Endocytosis impairement in *rab5ab* yolk morphants

Confocal video time-lapse of control and *rab5ab* YMOs (medium dose) soaked in Rhodamine B-Dextran for 5 minutes at sphere stage. 20 µm width stacks were captured every 4 minutes. Note the reduced dextran internalization ahead of the advancing EVL.

### Movie S4. Specific arrest of epiboly movements in *rab5ab* yolk morphants

Confocal video time-lapse of a membrane-GFP (Tg (β-*actin:m-GFP*) *rab5ab* YMOs (medium dose) that slowly proceeds throughout epiboly arresting at 70 % presenting an open back phenotype but succeeding in other gastrulation movements leading to somite formation.

### Movie S5. Medium dose *rab5ab* macroscopic phenotype

Macroscope video time-lapse of control and Rab5ab YMO sibling embryos (at a middle dose) are shown. Bright field images were captured every 5 minutes from sphere stage to 16 hours post fertilization. Note that the *rab5ab* YMO at a middle dose is at 60 % epiboly at the time when the control embryo closes (yellow arrow). The *rab5ab* YMO continues its elongation in the animal-vegetal direction but remains open.

**Movie S6. High dose *rab5ab* macroscopic phenotype**

Macroscope video time-lapse of control and Rab5ab YMO sibling embryos (at a high dose) are shown. Bright field images were captured every 5 minutes from sphere stage to 16 hours post fertilization. Note that *rab5ab* YMO at a high dose halt before reaching the equator and burst.

**Movie S7. Cortical Myosin flows on the E-YSL in control versus *rab5ab* YMOs**

Spinning-disc video time-lapses of zebrafish transgenic (Tg (β-*actin:MYL9L-GFP*)) embryos from 50% epiboly onwards (control sibling (top) and a *rab5ab* YMO (bottom). The movements of cortical actin were analyzed by Particle Image Velocimetry (PIV). 9 µm width stacks were captured every 12 seconds. Maximum projections are shown. Scale bar 25 µm. The retrograde animalward cortical myosin flows from the vegetal pole of the yolk towards the E-YSL are impaired in *rab5ab* YMOs.

**Movie S8. EVL marginal cells elongate in the CC direction in *rab5ab* YMOs**

Confocal video time-lapse of control and *rab5ab* yolk membrane labelled [Tg (*β-actin:m-GFP*)] zebrafish transgenic morphant embryos (medium dose). While control embryos marginal EVL cells elongate in the animal/vegetal direction (left), *rab5ab* YMOs marginal cells flatten and elongate in the circunferencial direction. The speed of progression of the EVL is reduced and eventually stalls.

**Movie S9. Yolk granules flows in *rab5ab* YMOs**

Flow trajectories from PIV measurements of a two-photon video time-lapse of a membrane-GFP (Tg (β-*actin:m-GFP*)) zebrafish transgenic *rab5ab* YMO at the middle plane, 350 µm deep inside, throughout epiboly. Scale bar 100 µm. Flows in the *rab5ab* YMO are partly arrested.

**Movie S10. Yolk granules kinematics in *rab5ab* yolk morphants**

Flow lines from PIV measurements of two-photon excitation stitched video time-lapses of membrane-GFP (Tg (β-*actin:m-GFP*)) zebrafish transgenic control (left) and *rab5ab*

(right) YMO siblings at the middle plane, 350 µm deep inside, throughout epiboly. Scale bar 100 µm. The *rab5ab* YMO shows epiboly delay and disrupted yolk flows.

**Movie S11. Power Density Maps in *rab5ab* yolk morphants**

Two-photon excitation video time-lapse of a membrane-GFP (Tg (β-*actin:m-GFP*)) *rab5ab* YMO at the middle plane, 350 µm deep inside, throughout epiboly (left). Mechanical power density maps were calculated by HR from the velocity fields, color-coded at an equal scale for each time point (right) and overlaid on the fluorescence images (negative - blue; 0 - green; positive - red) (middle). The relative mean square error for the Power is displayed as a percentage for each time point. Scale bar 100 µm. As in the wild type [2], during doming, most of the energy supply is generated by the blastoderm. After 50 % epiboly, the E-YSL constriction becomes the main motor of epiboly, while the EVL cells resist their stretching. Thus, *rab5ab* YMOs display no qualitative differences with wild type embryos in their mechanical activity distribution but, importantly, they exhibit an overall decrease of power of about four fold.

**Movie S12. Longitudinal and latitudinal stresses in *rab5ab* yolk morphants**

Main surface stresses were calculated by HR of velocity fields obtained from stitched two-photon excitation video time-lapse of a membrane-GFP (Tg (β-*actin:m-GFP*)) *rab5ab* YMO embryo at the middle plane, 350 µm deep inside, throughout epiboly . Longitudinal (red) and latitudinal (green) stresses and their differences (blue) were plotted as a function of the φ angle from animal to vegetal. Time points were every 40 minutes. The equator - dotted yellow line -, yolk surface - purple shadow - and the relative mean square error of the pressure as a percentage for each time point are displayed. In these morphants, the longitudinal and latitudinal stresses are equal at the poles. Contrary to wild type embryos, the latitudinal stress does not steep up from animal to vegetal. Their difference (longitudinal minus latitudinal) shows after 50 % epiboly a defined profile at the EVL margin, becoming positive in the EVL and negative at the E-YSL.